13th International Conference on
Steel, Space and Composite Structures
31 January - 2 February 2018, Perth, Australia

IMPACT OF A MOVING TROLLEY ON THE DYNAMIC RESPONSE OF A SHIP UNLOADER BOOM

Giulia Milana*†, Kian Banisoleiman* and Arturo González‡

*Lloyd's Register
Global Technology Centre, Southampton, UK.
giulia.milana@lr.org giulia.milana@ucdconnect.ie

Keywords: Ship unloader, Steel, Moving Load, Structures, Dynamics

Abstract. *Container cranes represent an important link in the maritime transport system. Assessment of residual life for such cranes is important both in terms of safety and cost of repair and maintenance. These cranes usually have a hoisting trolley system which can move along the boom for lifting, carrying and lowering the payload, loading/unloading vessels in the harbour. This paper investigates the dynamic response of the lifting boom using a non-linear finite element analysis. A number of such moving trolley systems, with different degrees of complexity, are modelled to assess the impact of their influence on the boom dynamic response parameters. Results from the finite element analysis are compared to a pseudo-static analysis and are presented in terms of a Dynamic Response Factor (DRF).*

1 INTRODUCTION

Ship unloaders (Fig. 1) play a crucial role in the handling of large amount of bulk materials that takes place in ports. Being exposed to continuous alternating stresses resulting from loading and unloading of bulk materials in an extremely aggressive environment, these structures are prone to rapid deterioration. This can ultimately lead to failure of either the stationary main structure, or moving mechanisms, if periodic inspection and repair is lapsed, with catastrophic safety implications.

Figure 1: Standard ship unloader and its main structural members.

‡University College Dublin, School of Civil Engineering, Dublin 4, Ireland.

One of main causes of failure is fatigue. This is significantly affected by the loading duty cycle in terms of numbers and the magnitudes of loading (hoisting) cycles and ambient weather (wind) conditions. The resulting stress range could progressively propagate minute subsurface cracks (material internal flaws) overtime to exhibit as larger visible/detectable hairline cracks at the material surface. In terms of capacity, fatigue life duration is also affected by wear, accidental damage to structural parts (geometry) and corrosion (plate thickness).

Further, as ship unloaders are often slender structures, with time-varying loading conditions, and minimal damping, influence of dynamic response should be considered, i.e., vibratory response, where number of fatigue cycles increase with higher dynamic excitation.

The standard procedure to evaluate the residual fatigue life, Federation Europeenne de la Manutention [1], is based on a pseudo-static analysis of the structure, comprising static analysis and application of Dynamic Coefficient Factor DCF (ψ), due to "oscillations caused when lifting the load by multiplying the loads due to working load by the factor ψ" [1] . DCF is defined in the Procedure [1] as the ratio of the maximum total load (= 'static' + 'dynamic') to the maximum static load effect, taking into account all possible positions of the load on the boom. For example, the Procedure [1] recommends DCF of 1.6, for overhead travelling and bridge cranes and 1.3 for jib cranes, once the hoisting speed goes beyond 1 m/s [2]. These DCFs are necessarily conservative to cover a wide range of boom moving trolley hoisting systems. However, some structural forms of ship unloaders are more sensitive to dynamic excitation than others. Therefore, the aim of this paper is to evaluate how a true transient dynamic analysis, coupling both structure and the moving trolley into one non-linear single system, compares to a pseudo-static or static analysis in terms of a Dynamic Response Factor (DRF), defined as ($dynamic_{peak\_to\_peak}$ + $static_{mean}$)/ $static_{mean}$ response, when subjected to the same load.

2 SIMULATION MODELS

2.1 Equivalent Model of the Boom

Zrnic et al. [3] note that the boom is the most representative structural element regarding the dynamic behaviour of the ship unloader. Therefore, the aim of this paper is to evaluate how a true transient dynamic analysis, coupling both structure and the moving trolley into one non-linear single system.

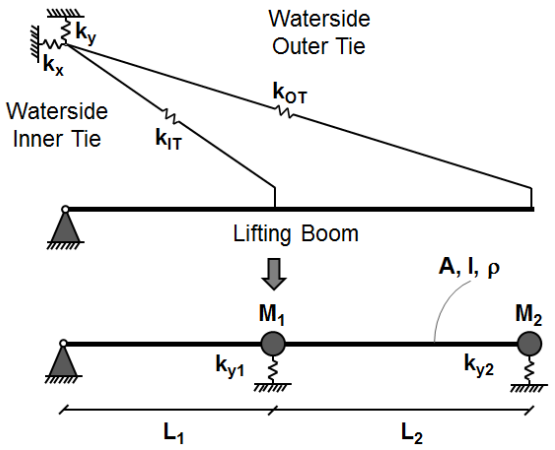

Figure 2: Equivalent model of the lifting boom (Adapted from Zrnic et al [3])

Based on Zrnic et al. [3], a two dimensional, 2D, non-linear Finite Element (FE) model of the boom (Fig. 2), was built using Euler Beams, Springs and Mass elements. The FE model was coded in MATLAB [4]. It consisted of 22 Beam elements, each of 3 m length. Three degrees of freedom (DoF) was considered at each beam node *x*, *y* and θ. The boom model was pin-jointed the left hand side, LHS of the boom. Two spring elements (in the vertical direction) K_{y1} and K_{y2} and concentrated masses M_1 and M_2 were modelled at the fist span, location 'L_1' and full span location '$L_1 + L_2$' from the LHS of the boom. The springs and masses simulated the influence of the ties on the structure of the boom.

Table 1 gives the values adopted for the model parameters.

A	0.1925 m^2	M_1	3690 kg
E	210,000 MN/m^2	M_2	21170 kg
I	0.2484389 m^4	K_{y1}	1.117462 10^7 N/m
ρ	9602.39 kg/m^3	K_{y2}	3.18675 10^6 N/m
L_1	30 m		
L_2	36 m		

Table 1: Data for building equivalent model of the lifting model, from Zrnic et al [3]

2.2 Interaction between Moving Load and the Boom

The general equation of motion for the global system was given by:

$$[M]\{\ddot{u}\} + [C]\{\dot{u}\} + [K]\{u\} = F(t) \quad (1)$$

Where,$[M]$,$[C]$ and $[K]$ were respectively the global mass, damping and stiffness matrices of the FE model, and $\{\ddot{u}\}$,$\{\dot{u}\}$ and $\{u\}$ were respectively the acceleration, velocity and displacement DOFs. The force vector $F(t)$ was expressed in terms of the shape function vectors as follows:

$$\boldsymbol{F(t)} = \boldsymbol{N_x(t)^T}\, P_x(t) + \boldsymbol{N_y(t)^T}\, P_y(t) \quad (2)$$

$P_x(t)$ and $P_y(t)$ were the applied forces in the *x* and *y* directions respectively, which could have different expressions depending on the adopted models of the moving trolley system as explained in Section 2.3 below.

$\boldsymbol{N_x(t)}$ and $\boldsymbol{N_y(t)}$ were the global shape function vectors that distributed the forces acting on an element to its DOFs. The shape functions, in the horizontal (*x)* direction and vertical direction (*y* and θ) components of displacement, were given by equations (4a) and (4b) respectively [5]:

$$\boldsymbol{N_x(t)} = \left[0 \;\; 0 \;\; 0 \;\; \ldots \;\; {N_1}^{(s)} \;\; 0 \;\; 0 \;\; {N_4}^{(s)} \;\; 0 \;\; 0 \;\; \ldots \;\; 0 \;\; 0 \;\; 0\right] \quad (4a)$$

$$\boldsymbol{N_y(t)} = \left[0 \;\; 0 \;\; 0 \;\; \ldots \;\; 0 \;\; {N_2}^{(s)} \;\; {N_3}^{(s)} \;\; 0 \;\; {N_5}^{(s)} \;\; {N_6}^{(s)} \;\; \ldots \;\; 0 \;\; 0 \;\; 0\right] \quad (4b)$$

The non-zero components in equations (4a) and (4b) correspond to the DOF of the element s, where the moving mass was located at time t. The shape functions were obtained from $x_m(t)$ using the following expressions [5]:

$$N_1 = 1 - \xi(t)\,;\;\; N_2 = 1 - 3\xi(t)^2 + 2\xi(t)^3\,;\;\; N_3 = [\xi(t) - 2\xi(t)^2 + \xi(t)^3]l \quad (5a)$$

$$N_4 = \xi(t)\,;\;\; N_5 = 3\xi(t)^2 - 2\xi(t)^3\,;\;\; N_6 = [-2\xi(t)^2 + \xi(t)^3]l \quad (5b)$$

with $(t) = \frac{x_m(t)}{l}$, where l was the length of each element and $x_m(t)$ was the distance from the left side closest node, given by:

$$x_m(t) = x_T(t) - (s-1)l \quad (6)$$

Equation (7) identifies the element number s on which the load is applied at time t.

$$s = integer\left(\frac{x_T(t)}{l}\right) + 1 \quad (7)$$

The time response of the system of equations (1) was obtained using Wilson Theta step-by-step integration method [6]. External damping was neglected ($[C] = [0]$) since ship unloader cranes are typically lightly damped [7].

2.3 Numerical Models of Moving Trolley System

The main dynamic phenomena in quayside container cranes are consequences of dynamic interaction between trolley, hanging load and crane's supporting structure (Zrnic et al [8]). In order to identify the parameters that mostly influence the dynamic response, different models of the moving system were introduced and analysed in increasing order of complexity.

Fig. 3 presents the models considered. The same overall load (weight) of 175 tonne was considered for all models. The hoisting (lifting and the lowering) dynamics were not considered as estimates were given in the Procedure [1]. These models comprised; (a) point load; (b) mass; (c) sprung mass; (d) two masses interconnected by a spring, and (e) pendulum as seen below.

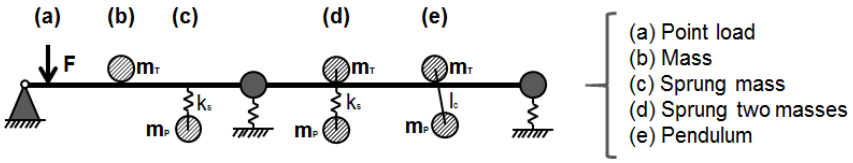

Figure 3: Moving trolley, load models.

Fig. 4 shows the two speed patterns considered for the moving trolley and load system. The speed of 6 m/s was the highest value reported in the literature for such moving trollies [9] and was used in this study. The first pattern, labelled 'Constant', was a constant speed of 6 m/s. The second schedule, referred to as 'Brake2', defined an initial constant speed of 6 m/s before braking at a constant deceleration of 1.2 m/s^2, coming to a stop at the right hand side, RHS, free end of the boom. The first constant speed assumption was justified, as when the moving trolley system was not in operation, it would be located at the landside (see Fig. 1). For a typical acceleration of 1.2 m/s^2, the moving trolley would achieve a speed of 6 m/s in 15 m, i.e., before reaching the waterside section of the boom considered (see Fig. 3).

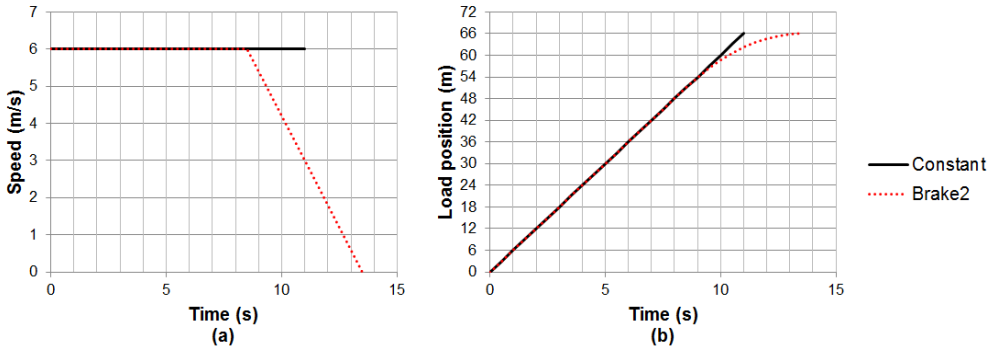

Figure 4: Speed patterns: (a) speed vs time and (b) load position vs time.

2.3.1 Point Load - Model (a) on Fig. 3

Equation (8) defines the forces applied by this simple model. Here, inertia effects interacting between the moving trolley (load) and the structure were ignored. This model allowed a preliminary assessment of the impact of the speed of the moving trolley on the boom in isolation. $P_x(t)$ and $P_y(t)$ in equation (2) were defined as:

$$P_x(t) = 0 \quad ; \quad P_y(t) = F \tag{8}$$

2.3.2 Mass - Model (b) on Fig. 3

In this case effect of inertia forces, in terms of Coriolis and Centripetal forces [6] acting on the moving trolley (load) and the boom were accounted for. Thus, expressions $P_x(t)$ and $P_y(t)$ were given by:

$$P_x(t) = -m_T(\ddot{w}_x(x_T,t) + \ddot{x}_T(t)) \quad ; \quad P_y(t) = m_T\big(g - \ddot{w}_y(x_T,t)\big) \tag{9}$$

Where, $\ddot{w}_x(x_T,t)$ and $\ddot{w}_y(x_T,t)$ represent the horizontal and vertical acceleration respectively of the moving trolley mass m_T at time t and $\ddot{x}_T(t)$ is the horizontal acceleration of the trolley at time t. In all models throughout this paper, the trolley mass m_T was assumed to be in permanent contact with the boom.

Equations (10a) and (10b) relate $w_x(x_T,t)$ and $w_y(x_T,t)$ to $w_x(x,t)$ and $w_y(x,t)$ which are the horizontal and vertical translations respectively of the boom at the contact point with the moving trolley mass m_T.

$$\frac{d^2w_x(x_T,t)}{dt^2} \approx \frac{\partial^2 w_x(x,t)}{\partial t^2} \tag{10a}$$

$$\frac{d^2w_y(x_T,t)}{dt^2} = \frac{\partial^2 w_y(x,t)}{\partial t^2} + 2\dot{x}_T(t)\frac{\partial^2 w_y(x,t)}{\partial x \partial t} + \dot{x}_T{}^2(t)\frac{\partial^2 w_y(x,t)}{\partial x^2} + \ddot{x}_T(t)\frac{\partial w_y(x,t)}{\partial x} \tag{10b}$$

The relationship between the horizontal $w_x(x,t)$ and vertical $w_y(x,t)$ translations and the nodal displacements of the boom $\{u\}$, were via the shape functions.

$$w_x(x,t) = N_x(t)\{u\} \quad ; \quad w_y(x,t) = N_y(t)\{u\} \tag{11}$$

Substituting Equations (10a), (10b) and (11) into Equation (9) yields:

$$P_x(t) = -m_T(N_x(t)\{\ddot{u}\} + \ddot{x}_T(t)) \tag{12a}$$

$$P_y(t) = m_T\big(g - (N_y(t)\{\ddot{u}\} + 2\dot{x}_T(t)N_y'(t)\{\dot{u}\} + \dot{x}_T{}^2(t)N_y''(t)\{u\} + \ddot{x}_T(t)N_y{}'(t)\{u\})\big) \tag{12b}$$

Where, $m_T 2\dot{x}_T(t)N_y'(t)\{\dot{u}\}$ was the Coriolis force, $m_T\dot{x}_T{}^2(t)N_y''(t)\{u\}$ was the Centripetal force and $m_T\ddot{x}_T(t)N_y{}'(t)\{u\}$ was the acceleration force exerted by the moving trolley mass on the boom. The equation of motion associated to the moving mass was obtained by replacing equations (12a) and (12b) into Equation (2), and then Equation (2) into Equation (1), as given by equation (13):

$$\big[\widetilde{M}\big]\{\ddot{u}\} + \big[\check{C}\big]\{\dot{u}\} + \big[\widetilde{K}\big]\{u\} = \tilde{F}(t) \tag{13}$$

where:

$$\big[\widetilde{M}\big] = \lfloor M \rfloor + m_T N_y(t)^T N_y(t) + m_T N_x(t)^T N_x(t)) \tag{14}$$

$$\big[\check{C}\big] = \lceil C \rceil + 2m_T\dot{x}_T(t)N_y(t)^T N_y{}'(t) \tag{15}$$

$$\big[\widetilde{K}\big] = [K] + m_T\dot{x}_T{}^2(t)N_y(t)^T N_y''(t) + m_T\ddot{x}_T(t)N_y(t)^T N_y{}'(t) \tag{16}$$

$$\tilde{F}(t) = m_T g N_y(t)^T - m_T\ddot{x}_T(t)N_x(t)^T \tag{17}$$

2.3.3 Sprung Mass and Sprung Masses - Models (c and d) on Fig. 3

In the case of a moving sprung mass and sprung masses connected by a linear spring, an additional independent DOF was introduced for the vertical displacement of the payload. The system of equations governing the problem was given by [11].

$$\begin{cases} [M]\{\ddot{u}\} + \lceil C \rceil\{\dot{u}\} + [K]\{u\} = F(t) \\ m_P\ddot{y} + k_s\big(y - w_y(x_T,t)\big) = 0 \end{cases} \tag{18}$$

Where y was the absolute vertical displacement of the sprung payload mass m_P and for the single mass, k_s was the stiffness of the linear spring connecting the payload mass to the boom.

In the case of two masses, the linear spring k_s connected the payload mass m_P to the trolley mass m_T moving on the boom. In this case the inertia forces were given by Equation 15 [12].

$$P_x(t) = -(m_T + m_P)(\ddot{w}_x(x_T,t) + \ddot{x}_T(t)) \quad ; \quad P_y(t) = m_T\big(g - \ddot{w}_y(x_T,t)\big) + m_P(g - \ddot{y}) \tag{19}$$

Substituting Equations (19) into Equation (2), and subsequently into Equation (18), the equations of motion associated to the sprung mass becomes Equation (20).

$$\begin{bmatrix} \lfloor M \rfloor + [M_1] & 0 \\ 0 & m_P \end{bmatrix}\begin{Bmatrix} \{\ddot{u}\} \\ \ddot{y} \end{Bmatrix} + \begin{bmatrix} \lceil C \rceil + [C_1] & 0 \\ 0 & 0 \end{bmatrix}\begin{Bmatrix} \{\dot{u}\} \\ \dot{y} \end{Bmatrix} + \begin{bmatrix} [K] + [K_1] & -k_s N_y{}^T \\ -k_s N_y & k_s \end{bmatrix}\begin{Bmatrix} \{u\} \\ y \end{Bmatrix} = \begin{Bmatrix} (m_{TOT})(g N_y{}^T - \ddot{x}_T N_x{}^T) \\ 0 \end{Bmatrix} \tag{20}$$

where:

$$\lfloor M_1 \rfloor = m_T N_y(t)^T N_y(t) + (m_T + m_P)N_x(t)^T N_x(t) \tag{21}$$

$$\lceil C_1 \rceil = 2m_T\dot{x}_T(t)N_y(t)^T N_y{}'(t) \tag{22}$$

$$[K_1] = m_T\dot{x}_T{}^2(t)N_y(t)^T N_y''(t) + m_T\ddot{x}_T(t)N_y(t)^T N_y{}'(t) + k_s N_y(t)^T N_y(t) \tag{23}$$

$$m_{TOT} = m_T + m_P \tag{24}$$

It can be seen that the sprung single payload mass model, was a particular case of the two sprung mass model, where the trolley mass m_T was equal to zero.

2.3.4 Pendulum - Model (e) on Fig. 3

This was a suspended (free pendulum) payload mass m_P connected with an infinitely stiff cable of length l_c to the moving trolley mass m_T on the boom, which could be excited for example by horizontal/lateral wind forces. There are a number of approaches towards

modelling the action of a pendulum (Oguamanam et al [13], Yazid [14] and Wu [15]). The Wu [15] model (Fig. 5) was used where the swinging payload mass was modelled as an equivalent payload mass $m_{eq}(t)$, depending on the pendulum angle $\theta(t)$, subtended from the vertical.

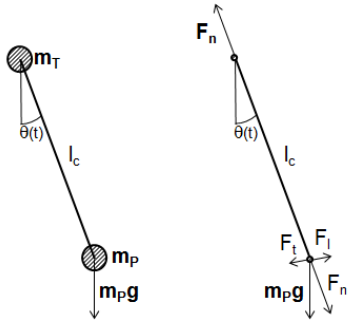

Figure 5 : Diagram of the moving system and force components (Adapted from Wu [15]).

The vertical force of the payload mass $m_P\ g$ on the pendulum was resolved into two components F_n and F_t, normal and tangential to the pendulum. At small swing angles θ_A, the tangential component F_t was balanced by the inertial force F_I of the swinging object. Thus, the only force component transferred at the contact point between the beam and the moving system was F_n. The value of $m_{eq}(t)$ was obtained by resolving F_n into the vertical direction as follows. Resolving F_n in the horizontal direction, the term $m_P g \cos\theta(t) \sin\theta(t)$ is obtained as part of the external horizontal force (Eq. 28).

$$m_{eq}(t) = m_T + m_P \cos^2\theta(t) \tag{25}$$

Where, the swinging angle $\theta(t)$ is in the form:

$$\theta(t) = \theta_A \cos\bar{\omega}t \quad ; \quad 0° < \theta_A \leq 20° \tag{26}$$

θ_A was the pendulum angular displacement and $\bar{\omega}$ the natural frequency, which was assumed to be the natural frequency of a simple pendulum given by Equation (27) as there was no other forcing functions acting on the pendulum.

$$\bar{\omega} = \sqrt{g/l_c} \tag{27}$$

Where, g was gravity and l_c was the length of the pendulum.

The terms for $P_x(t)$ and $P_y(t)$ for pendulum were given by Equation (28):

$$P_x(t) = -m_{eq}(\ddot{w}_x(x_T,t) + \ddot{x}_T(t)) + m_P g \cos\theta(t) \sin\theta(t) \ ; \quad P_y(t) = m_{eq}\big(g - \ddot{w}_y(x_T,t)\big) \tag{28}$$

3 RESULTS

3.1 Natural Frequencies and Mode Shapes

Initially, the Eigen value and Eigen vectors of the boom model were evaluated without the moving trolley mass to compare against those published by Zrnic et al [3]. Table 2 compares the frequencies obtained for the first 5 vertical modes. It can be seen that in comparison with Zrnic et al [3] maximum differences below 1%.

Natural frequencies	Zrnic et al [3] (Hz)	FE model (Hz)	Difference (%)
I	1.46	1.45	0.26
II	3.22	3.21	0.37
III	8.48	8.43	0.58
IV	17.85	17.74	0.58
V	31.58	31.38	0.62

Table 2: Comparison of boom models, only natural frequencies in vertical *y* direction.

The mode shapes for the first three natural frequencies are presented below (Fig. 6A). It can be seen that mode-I was the 0-node bending mode of the boom and modes II and III were the 1 and 2 node bending modes respectively.

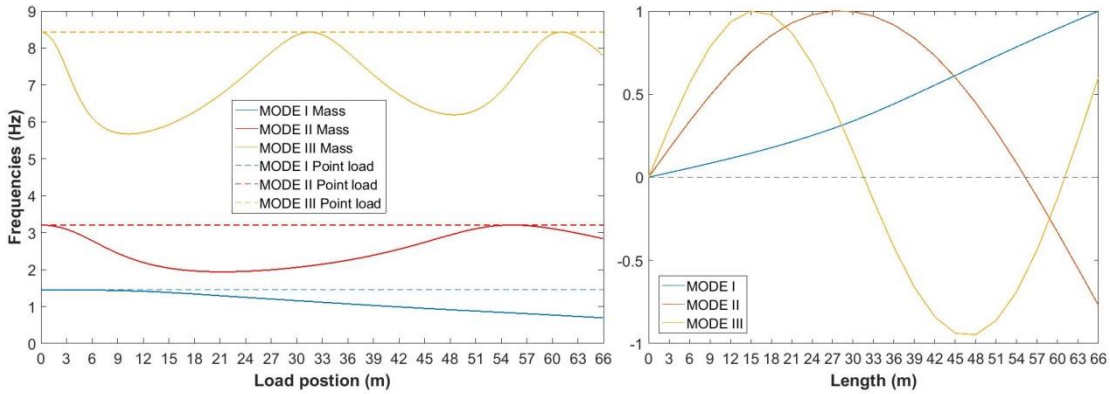

Figure 6: (A) First three mode shapes of the boom, in vertical *y* direction; (B) First three natural frequencies of the boom WRT position of the trolley on the boom; for Point Load model (dash lines) and Mass models of trolley.

Presence of the moving trolley (mass) modified the boom natural frequencies depending on the trolley position (Fig 6B), whereas modelling the effect of trolley mass (as point load) did not alter the boom natural frequencies.

It can be seen (Fig.6B) that when the trolley mass was at a modal node (zero modal displacement, Fig 6A) the natural frequency of the combined 'trolley & boom' system was the same as the 'boom only'. However, natural frequency of the 'trolley & boom' system was lower (due to Coriolis damping effects) than the 'boom only', at trolley locations corresponding to peak modal displacements, representing locations of peak vibration velocity.

3.2 Transient response

The transient response characteristics of the different trolley models are presented in the following sections. In all cases transient response is compared with that of the static case to derive the DRF for the boom. The static response of the boom was a special case of the transient analysis, i.e. at a very low trolley speed of (0.01 m/s), avoiding any oscillatory response.

3.2.1 Point Load - Model (a) on Fig. 3

Fig. 7 compares the transient oscillatory vertical displacement response of the first mid-span of the boom (at $L_1/2$=15m from LHS of boom) at three different constant trolley speeds (2, 6 and 10 m/s) with the static response.

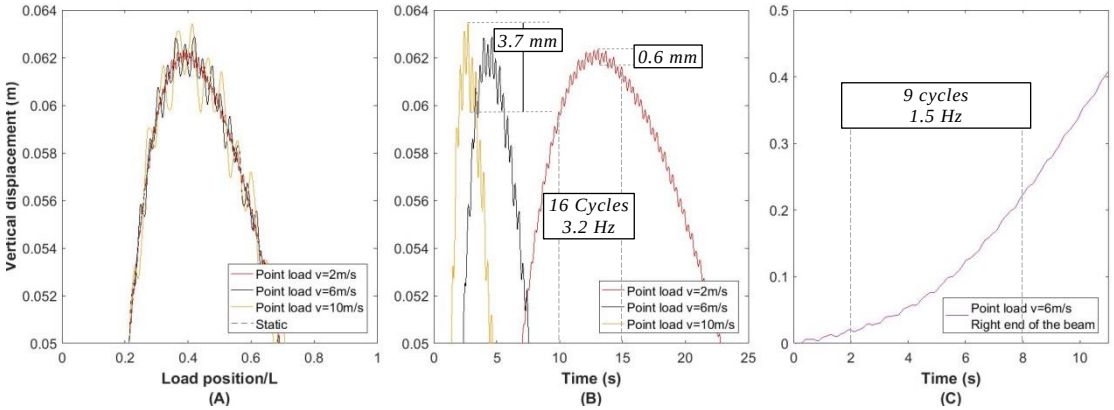

Figure 7: Mid-span vertical displacement of the first span versus: (A) load position, (B) time & (C) RHS of boom vertical displacement versus time at trolley speed of 6 (m/s).

Fig. 7A shows the resulting oscillatory response of the boom around the mean static deflection at $L_1/2$ as the trolley moved along the boom. Fig.7B shows the same oscillatory response against time, highlighting the mode-II response (at 3.21 Hz) at this location, where the modal displacement of mode-II was dominant.

Fig. 7C shows the transient response at the right hand end of the beam against time, with a trolley speed of 6 m/s. It shows that the mean vertical displacement increased against time as the trolley moved to the RHS of the boom. Further, it can be seen that the oscillatory response at this location was dominated by mode-I response (at 1.45 Hz).

DRF values of 1.01 (0.6/62+1=1.01), 1.03 and 1.06 (3.7/62+1=1.06) were obtained at 2, 6 and 10 m/s respectively.

3.2.2 Mass - Model (b) on Fig. 3

Fig. 8 shows the transient vertical and horizontal displacement of the first mid-span of the boom (at $L_1/2$=15m from LHS of boom) at a range of ratios m_T/M: 0.4, 0.8, 1.2, 1.6, where M was mass of the boom and m_T was the mass of the trolley and the payload, at the trolley speeds 6 m/s 'Brake2' pattern.

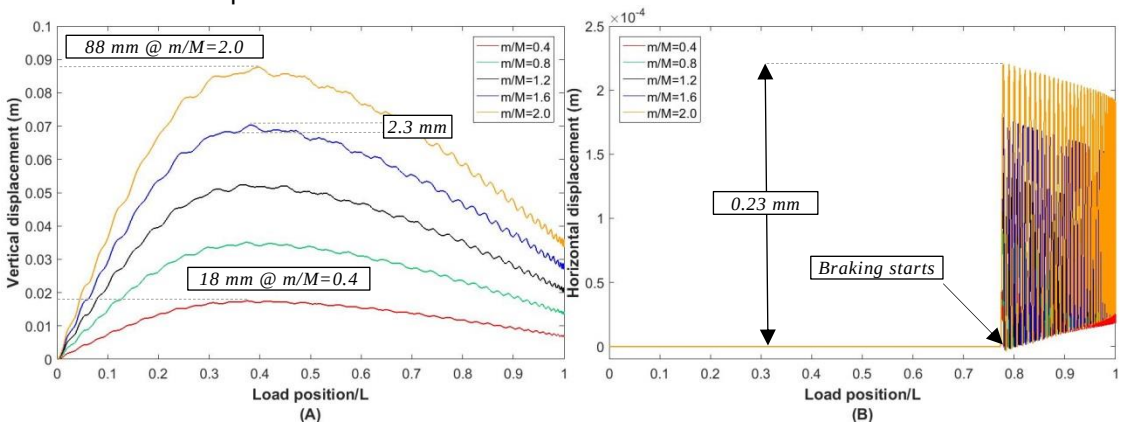

Figure 8: Mid-span (a) vertical and (b) horizontal displacements of the first span, for 'Brake2' speed pattern) and different mass ratios.

Fig. 8A shows the transient response of the boom (at $L_1/2$) in the vertical direction. It can be seen that in cases with heavier payload (higher m_T/M *ratio)* both the mean and the dynamic oscillatory response where higher than those at lower loads. DRF of vertical displacement were 1.028, 1.030, 1.031, 1.034 (2.3/69+1=1.034) and 1.035 for m_t/M of 0.4, 0.8, 1.2, 1.6 and 2.0 respectively.

Fig. 8B shows the transient response of the boom (at $L_1/2$) in the horizontal direction. It can be seen that a vibratory response appeared throughout the breaking period, but the total amplitudes (0.23 mm) were low compared to those in the vertical direction (88 mm).

3.2.3 Sprung Mass & Sprung Masses - Models (c & d) on Fig. 3

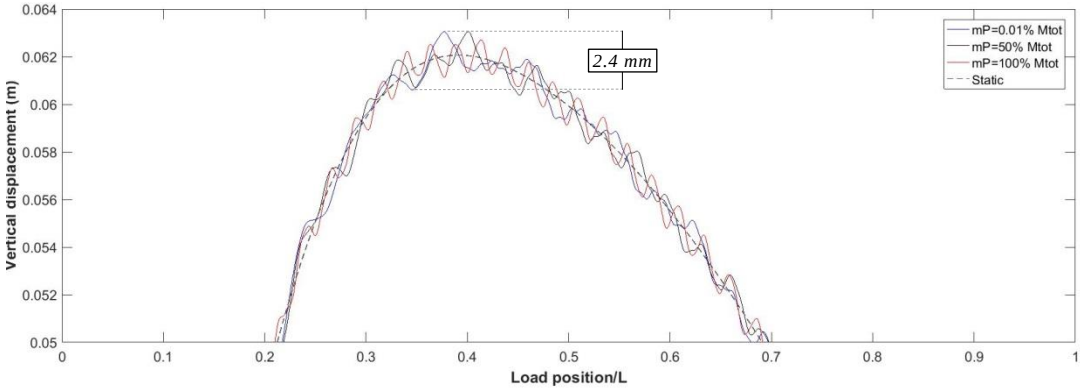

Figure 9: First mid-span vertical displacement of the first span, for two moving masses interconnected by a spring and different ratios of these masses.

Fig. 9 shows the transient response of the first mid-span of the boom (at $L_1/2$=15m from LHS) in the vertical direction, at a range of ratios m_p/M_{tot}: 0.1%, 50% and 100%, where m_p was the mass of payload and $M_{tot}=m_p + m_t$, was the combined mass of payload and the trolley, at a

constant speed of 6 m/s with 'Brake2' pattern. In these simulations the value of M_{tot} was a constant at 175 tonne, thus, the cases with the m_p/M_{tot} ratio at100% and 50% represented the sprung mass and sprung masses, system models (c) and (d) respectively.

DRF of vertical displacement were 1.022, 1.026 and 1.039 (2.4/62+1=1.039) at m_p/M_{tot} of 0.1%, 50% and 100% respectively.

3.2.4 Pendulum - Model (e) on Fig. 3

A pendulum length of l_c = 2 m was used and results were computed at range of swing angle θ_A values of 1, 5, 10, 15 and 20 degrees.

Fig. 10A and 10B show the transient response of the first mid-span of the boom (at $L_1/2$=15m from LHS) in the vertical and horizontal directions against time respectively, at a constant trolley speed of 6 m/s. It can be seen that the total amplitude of the vertical response was approximately 63 mm compared to a total horizontal response of 0.20mm. The oscillatory pendulum response at the frequency ($f = \sqrt{9.81/2}/2\pi = 0.35\ Hz$) was apparent in both vertical and horizontal response, with the latter comprising entirely of the pendulum response, whereas in the former the vibratory response was a synthesis of that of the pendulum and the mode-II (3.21 Hz) response at this location. Peak to peak vertical vibratory response was 4.9 mm.

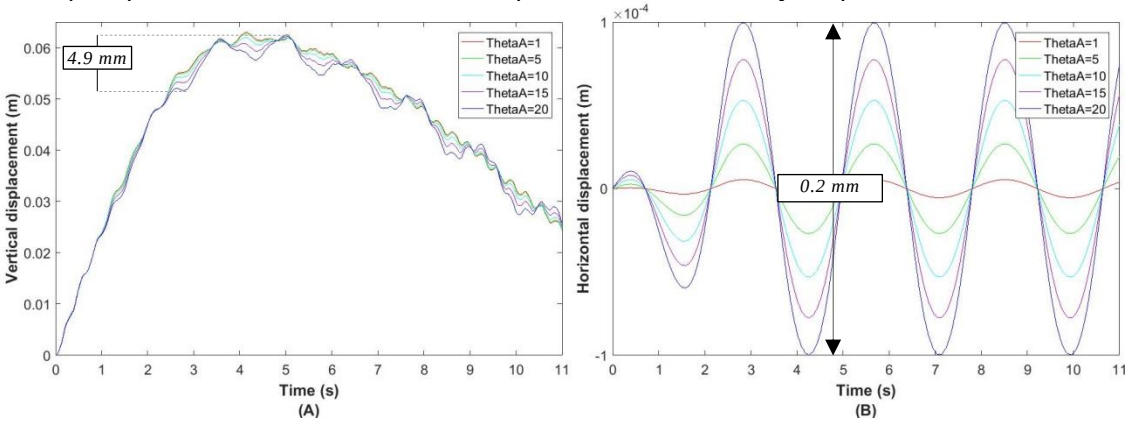

Figure 10: First mid-span transient response against time at different swing angles and constant trolley speed of 6 m/s, against time. (A) Vertical direction and (B) Horizontal direction.

DRFs in the vertical direction were 1.039, 1.036, 1.026, 1.048 and 1.08 (4.9/62+1=1.08) at θ_A of 1, 5, 10, 15 and 20 degree respectively.

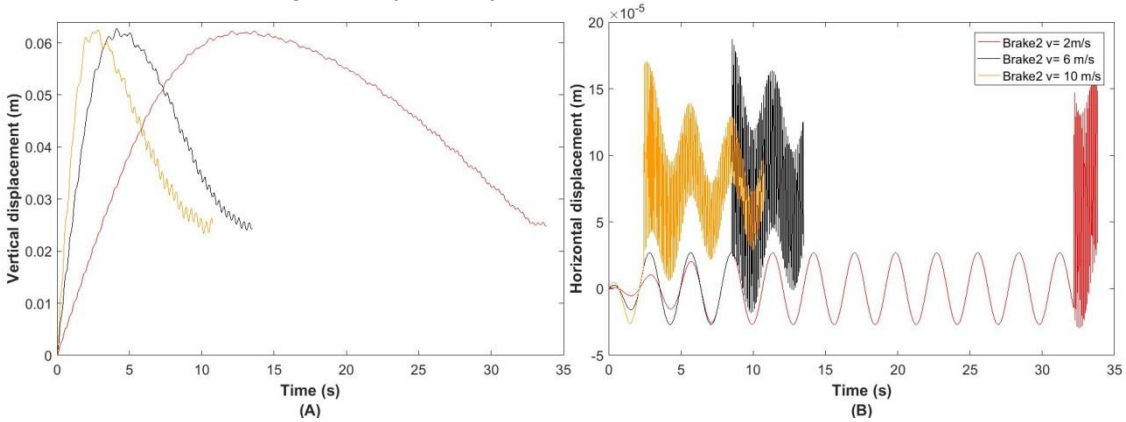

Figure 11: First mid-span transient response against time at different at different trolley speeds pendulum swing angles θ_A= 5° and different trolley speeds with Brake2 schedule, against time. (A) Vertical direction and (B) Horizontal direction.

Fig. 11A and 11B show the transient response of the first mid-span of the boom (at $L_1/2$=15m from LHS of boom) in the vertical and horizontal directions against time respectively, at a constant trolley speed of 2, 6 and 10 m/s with the 'Brake2' schedule., at θ_A of 5 degree. DRFs in the vertical direction were 1.011, 1.036 and 1.059 at trolley speeds of 2, 6 & 10 m/s with Brake2 schedule respectively, and at a swing angle of θ_A of 5 degrees.

4 CONCLUSIONS

This paper has presented the total vertical and horizontal response of the first mid-span of a ship unloader boom, when traversed by a moving trolley system based on a non-linear transient response analysis of the boom and the moving trolley. Five different models of the moving trolley were presented and parametric studies were carried out to assess the DRF relative to a static analysis. It has been shown that for the models of trolley systems in where there is a mass in permanent contact with the beam (mass, sprung two masses and pendulum) the natural frequencies of the boom in each mode is a function of the location of the trolley on the boom due to the Coriolis damping effects.

Braking initiated the horizontal response of the boom, but the amplitude (total response) was less than 1mm. Braking did not affect the dynamic response in the vertical direction. Total response in the vertical direction was significantly larger than in the horizontal direction, peaking at about 88 mm (Fig 8A), at the first mid-span when lifting a heavy weight at m_T/M *ratio* =2.0 twice the mass of the boom. DRF in the vertical direction was evaluated with a maximum value of 1.08 for pendulum, at a constant speed of 6 m/s and θ_A of 20 degree and a minimum value of 1.01 for a point load at a constant speed of 2 m/s.

ACKNOWLEDGEMENTS

This project has received funding from the European Union's Horizon 2020 research and innovation programme under the Marie Skłodowska-Curie grant agreement No. 642453 (http://trussitn.eu).

REFERENCES

[1] Federation Europeenne de la Manutention (FEM). Revised 1987.1.001. Rules for the Design of Hoisting Appliances. 3rd Edition.

[2] G. Milana, K. Banisoleiman and A. Gonzalez, *Field characterization of location-specific dynamic amplification factors towards fatigue calculations in ship unloaders*, 27th European Safety and Reliability Conference (ESREL2017), Portoroz, Slovenia (2017).

[2] N.D. Zrnic, K. Hoffmann and S.M. Bosnjak, *Modelling of dynamic interaction between structure and trolley for mega container cranes*, Mathematical and Computer Modelling of Dynamical Systems, (2009), 15.

[4] MATLAB Release 2016a, The MathWorks, Inc., Natick, Massachusetts, United States.

[5] V. Gasic, N. Zrnic and M. Milovancevic, Considerations of various moving load models in structural dynamics of large gantry cranes, FME Transactions, (2013), 41, 311-316.

[6] J.W. Tedesco, W.G. McDougal and C.A. Ross, Structural dynamics: theory and applications, Pearson, (1998).

[7] E.M. Abdel-Rahman, A.H. Nayfeh, and Z.N. Masoud, *Dynamics and control of cranes: a review*, Journal of vibration and control (2003), 9, 863–909.

[8] N. Zrnic, D. Oguamanam and S. Bosniak, *Dynamics and modelling of mega quayside container cranes*, FME Transactions, (2006), 34, 193-198.

[9] N.D. Zrnic, S.M. Bosnjak and K. Hoffmann, Parameter sensitivity analysis of non-dimensional models of quayside container cranes, Mathematical and computer modelling of dynamical systems (2010), 16, 145-160.

[10] I. Esen, Dynamic response of a beam due to an accelerating moving mass using moving finite element approximation, Mathematical and computational applications, (2011), 16, 171-182.

[11] V. Gasic, N. Zrnic A. Obradovic and S. Bosnjak, Considerations of moving oscillator problem in dynamic responses of bridge cranes, FME Transactions, (2011), 39, 17-24.

[12] N.D. Zrnic, V.M. Gasic and S.M. Bosnjak, Dynamic responses of a gantry crane system due to a moving body considered as moving oscillator, Archives of civil and mechanical engineering, (2015), 15, 243-250.

[13] D.C.D. Oguamanam, J.S. Hansen and G.R. Heppler, *Dynamic response of an overhead crane system*, Journal of sound and vibration (1998), 213(5), 889-906.

[14] E. Yazid, Mathematical modeling of a moving planar payload pendulum on flexible portal framework, Journal of mechatronics, lectrical power, and vehicular technology, (2011), 02, 99-104.

[15] J.J. Wu, Transverse and longitudinal vibrations of a frame structure due to a moving trolley and the hoisted object using moving finite element, International journal of mechanical sciences, (2008), 50, 613-625.